Research Square

Preprints are preliminary reports that have not undergone peer review.
They should not be considered conclusive, used to inform clinical practice,
or referenced by the media as validated information.

Evaluation of impact resistance for resistance-welded composites

J. F REIS

jonas.frank@unesp.br

São Paulo State University (UNESP)

T. S. R. Santos

São Paulo State University (UNESP)

L. F. B. MARQUES

São Paulo State University (UNESP)

L. F. SANTOS

São Paulo State University (UNESP)

L. R. O. HEIN

São Paulo State University (UNESP)

E. C. BOTELHO

São Paulo State University (UNESP)

Research Article

Keywords: Thermoplastic composites. Impact resistance. Compression after impact (CAI). Resistance welding

Posted Date: May 9th, 2026

DOI: https://doi.org/10.21203/rs.3.rs-9439570/v1

License: This work is licensed under a Creative Commons Attribution 4.0 International License.
Read Full License

Additional Declarations: No competing interests reported.

Abstract

This study investigates the impact resistance and damage tolerance of resistance-welded carbon (CF/PEI) and glass fiber (GF/PEI) thermoplastic composites. Specimens were subjected to 5J impacts, simulating Barely Visible Impact Damage (BVID), and 30J impacts representing severe structural damage. Quantitative results from Compression After Impact (CAI) tests revealed that CF/PEI maintains superior structural integrity under low-energy impacts, exhibiting a 14.41% increase in residual compressive strength (from 95.36 MPa to 109.10 MPa). This "self-reinforcing" behavior is attributed to the stainless-steel heating element (HE) acting as a high-stiffness interlayer that redistributes impact energy through elastic dissipation. Conversely, GF/PEI showed a 17.28% reduction under the same conditions. At 30 J, both materials experienced significant degradation, with strength reductions of 7.94% for CF/PEI and 26.29% for GF/PEI. The higher energy absorption of GF/PEI (25.5% greater than CF/PEI at 30J) is driven by irreversible damage, including extensive matrix cracking and radial fractures that compromise fiber lateral stability. These findings suggest CF/PEI is better suited for primary structures like Urban Air Mobility airframes, while GF/PEI is ideal for energy-shielding applications like electric vehicle battery enclosures. Finally, the results reinforce the viability of electrical resistance welding for structural thermoplastic composites.

1. Introduction

In recent years, the adoption of lightweight materials in structural applications throughout the transportation industry, especially in aviation, has grown rapidly. Improved fuel efficiency, lower costs, reduced environmental impact, enhanced performance, and compliance with regulatory standards fuel this trend [1, 2].

Furthermore, the transportation industry is dedicated to tackling emerging challenges posed by international regulations that require developing energy-efficient strategies to lower greenhouse gas emissions contributing to global warming. The lightweight nature of materials has become a crucial factor in this sector because of its ability to reduce energy consumption throughout the operational lifecycle of vehicles [3, 4].

The quest for lighter vehicles that do not compromise high mechanical performance remains one of the main challenges facing engineers and researchers today. The primary goal is to ensure safe transportation while also maintaining energy efficiency. Various strategies have been implemented to achieve this, particularly in reducing the weight of structural components through advanced material selection and design optimization [4].

Lightweight design and the use of innovative materials, such as composites and aluminum alloys, are recognized as effective strategies for structural applications and sustainable manufacturing [2]. The increasing use of advanced polymer matrix composites in lightweight structural applications has been primarily driven by their high specific strength, superior corrosion resistance, and improved fatigue

performance compared to conventional metals and alloys. This trend is particularly noticeable in the aerospace, automotive, and wind energy industries [5, 6].

Among the practical objectives of using fiber-reinforced thermoplastic composites (FRTCs) in these industrial sectors is to achieve high impact resistance with low specific weight. This reduction in weight lowers fuel consumption and promotes a more sustainable approach, allowing for the design of modeled transverse load-bearing structures [7, 8].

Although thermoset composites dominate most applications, the growing interest in thermoplastic composites is driven by their enhanced damage tolerance [9], shorter processing cycles [10], and recyclability [11].

Additionally, their weldability is a significant factor in the rising use of thermoplastic composites in industrial sectors, particularly in the aerospace industry. This capability stems from the intrinsic property of thermoplastic matrices, which can be melted or softened upon heating [12]. Although this melting or softening reduces molecular mass, thermoplastics retain their original mechanical properties after cooling [12, 13].

Welding of thermoplastic composites requires heating the joint interface above the polymer's glass transition temperature (Tg, for amorphous polymers) or melting temperature (Tm, for semi-crystalline polymers) to allow interdiffusion of polymer chains across the interface. The joint is then consolidated under pressure during cooling [6, 14].

Welding is a more suitable technology for joining thermoplastic composites than mechanical fastening or adhesive bonding [15]. Among the various welding techniques available today for the assembly and repair structural polymer composites, resistance welding has emerged as one of the most efficient and promising methods. This is due to its advantages, which include low operational costs, processing simplicity, and suitability for large-scale structures in a semi-continuous process (e.g., aircraft wings) [16, 17].

However, a key challenge preventing the widespread use of composite laminates or sandwich structures, especially in multi-component systems, is the joining interfaces. These joint regions create structural discontinuities that are susceptible to stress concentrations, which can result in premature fracture [1]. Moreover, there is limited experimental knowledge of the failure mechanisms governing welded joints [18].

According to Aloamari et al. [19], a significant challenge hindering the adoption of fiber-reinforced composites in the aerospace and automotive industries is the inherent risk of foreign object impact on structural components. Specifically, low-velocity impacts from debris or dropped tools can inflict internal damage that significantly compromises the mechanical strength of the composite. Visual inspection often does not detect such damage, raising serious safety and durability concerns [20, 21].

Low-velocity impact (LVI) tests on glass and carbon fiber-reinforced composites indicate that the stacking sequence of layers and laminate thickness significantly influence energy absorption and stress distribution. However, analyzing absorbed energy and impact velocities alone is insufficient to characterize the failure mechanisms in welded joints fully. To comprehensively assess damage evolution and identify failure modes, a post-impact analysis of the damaged specimen, including techniques such as microscopy, ultrasonic inspection, or computed tomography, is essential [19].

The literature documents several well-established techniques for post-impact analysis. For instance, visual inspection can assess specific damage types in impacted specimens, such as fiber failure and delamination. Additionally, correlating detected damage volumes with absorbed energy through optical measurements, such as 3D scanning or digital image correlation, is widely used for estimating impact effects in composite materials [22, 23].

While thermoplastic composites offer high damage tolerance and recyclability, the joining interfaces remains a critical challenge for structural assembly. These regions create structural discontinuities susceptible to stress concentrations. Although resistance welding is an efficient joining method, the insertion of a metallic heating element (HE) introduces a distinct material interface that governs the failure mechanisms. There is currently limited experimental knowledge regarding how these welded joints behave under low-velocity impact (LVI) and their subsequent residual strength. This study addresses this gap by identifying the primary fracture modes and characterizing the mechanical behavior of welded CF/PEI and GF/PEI under impact conditions.

This study aims to fabricate welded samples of glass fiber-reinforced polyether imide (GF/PEI) and carbon fiber-reinforced (CF/PEI) composites to determine and identify the primary fracture modes these materials undergo. To achieve this, impact testing and post-impact compression analysis will be conducted. Optical microscopy will then be employed to analyze and characterize the mechanical behavior of these materials under fracture conditions, thereby contributing to the existing body of knowledge in the field.

2. Materials and methods

2.1 Materials

The thermoplastic laminates used in this study were made of PEI matrix composites reinforced with GF and CF, supplied by Toray Advanced Composites. The laminates were fabricated with a [(0/90)]5s stacking sequence using hot compression molding with controlled heating and cooling cycles to ensure matrix consolidation. The composite configuration included approximately 50% fiber volume fraction and 0.5% porosity. Typically, the laminate is produced using molds and processed from semi-preg systems through the hot compression molding technique, utilizing controlled heating and cooling cycles. Table 1 presents a summary of PEI's key properties, as provided by Toray Advanced Composites.

Table 1
Key properties of PEI (polyetherimide).

Tg	Melt temperature	Tensile strength	Tensile modulus	Compression strength
215°C	300°C	105 MPa	3,276 MPa	152 MPa

2.2 Welding process

The resistance welding of composite materials was performed at São Paulo State University (UNESP), Department of Materials and Technology. The parameters used in the study (45A current, 80s time, and 0.7 MPa pressure) were based on the work of Reis et al. [24]. The HE used was a 304 stainless steel mesh, with 200 mesh, diameter/wire ratio of 0,058 and aperture of 0,069 mm.

2.3 Impact resistance testing

The impact resistance tests were performed at the Institute of Technological Research (LEL/IPT) in São José dos Campos/SP, utilizing an Instron CEAST testing machine equipped with a spherical penetrator and a dart-type impactor (Fig. 1). During the tests, a data acquisition system recorded all energies absorbed by the impacted specimens. The specimens measured 150 mm in length, 100 mm in width, and 4.1 to 4.9 mm in thickness. Testing was conducted at 5 J and 30 J energy levels according to ASTM D7136-20, with five specimens evaluated for each processing condition. The energy levels of 5J and 30J were selected to represent two critical service scenarios: 5J simulates Barely Visible Impact Damage (BVID), such as dropped tools during maintenance, while 30J represents severe structural damage to evaluate the propagation limit of interlaminar delamination at the welded interface.

2.4 Compression After Impact testing (CAI)

Compression After Impact (CAI) testing was conducted using an MTS Landmark model 370.25 universal testing machine. Following ASTM D7137-17, three specimens per processing condition, each previously subjected to impact resistance testing and maintaining identical dimensions, were evaluated to determine the reduction in compressive strength caused by the impact damage. The tests were conducted at the Institute for Technological Research (LEL/IPT) in São José dos Campos/SP. CAI testing was chosen because it is the most sensitive method for evaluating damage tolerance in composite laminates. Composites are inherently susceptible to compressive loads due to fiber microbuckling [25]. In resistance-welded joints, impact-induced delamination at the heating element interface drastically reduces the lateral stability of the layers. Since compression forces these damaged interfaces into instability, it serves as the most rigorous test to evaluate the integrity and reliability of the welded union post-impact.

2.5 Optical characterization

Optical microscopy was conducted using a Zeiss Axio Imager Z2m microscope. Image mapping techniques were utilized under bright and dark-field illumination modes, along with extended depth-of-

field (EDOF) reconstruction. The SEM was performed using a JEOL JSM 6360 instrument with a secondary electron detector.

3. Results and discussion

3.1 Impact results

Figure 2 illustrates the global impact response at two energy levels (5 J and 30 J) through force-time, force-displacement, velocity-time, and displacement-time curves for welded CF/PEI and GF/PEI laminates.

The CF/PEI laminate demonstrated a substantial increase in peak force as the impact energy rose from 5 J to 30 J (Fig. 2a). The oscillations observed in the CF/PEI force-time curves at 30 J (Fig. 2a) indicate progressive failure events, including matrix cracking, delamination, and sequential fiber fracture. This behavior was anticipated, as higher impact energy results in greater momentum transfer to the laminate, leading to increased impact force. The oscillations observed in the post-peak force curves, particularly at 30 J, suggest the presence of progressive damage mechanisms, such as delamination and fiber fractures [26, 27]. This observation indicates that multiple damage events have occurred, including delamination. Delaminations propagate due to high transverse shear stresses near the impacted surface. The damage progresses into other failure modes, leading to significant fiber damage that further evolves into fiber fracture and pull-out [28]. The stainless-steel mesh embedded in the welded joint may influence crack propagation and energy absorption during impact [29], altering the force-time curve profile. The GF/PEI laminate exhibited smoother post-peak behavior in the force-time curves (Fig. 2b), showing fewer oscillations than CF/PEI, suggesting a less complex fracture process and a lower incidence of delamination. The greater fracture displacement observed for GF/PEI (Fig. 2d) indicates increased ductility, contributing to improved energy absorption during impact. The larger area beneath the force-displacement curve at the 30 J impact energy level demonstrates the material's capacity to absorb more energy during higher-intensity impacts.

3.2 Compression After Impact testing results

Incorporating stainless steel mesh into the welded joint positively influenced the energy absorption capacity of the laminates. The mesh acted as localized reinforcement, restricting crack propagation and redistributing impact energy to the surrounding areas of the material, consistent with observations by Mandegarian and Hojjati [29] and Sakthivel and Vijayakumar [30]. Additionally, the HE acts as a localized reinforcement, increasing joint strength, limiting crack propagation, and improving stress distribution by transferring impact energy to the surrounding areas of the material [30–32]. However, welding can induce microstructural changes in the laminate, such as polymer matrix degradation. Amorphous polymers like PEI absorb moisture, which can lead to void formation during heating and negatively impact the joint's mechanical performance, as Cengiz et al. [31] reported, potentially compromising impact resistance. Table 2 presents the compressive strength (F_{CAI}) values obtained, and Fig. 3 depicts the post-impact behavior of GF/PEI and CF/PEI materials.

Table 2
Values of F_{CAI}.

Condition	Compressive strength (MPa) ± σ_M
Carbon fiber without impact (Base)	95.36 ± 10.92
Carbon fiber impact- 5J	109.10 ± 5.52
Carbon fiber impact- 30J	87.79 ± 16.93
Glass fiber without impact (Base)	79.55 ± 18.27
Glass fiber impact- 5J	65.80 ± 2.31
Glass fiber impact- 30J	58.64 ± 2.54

The values in Table 2 illustrate distinct behaviors between CF/PEI and GF/PEI composites when subjected to varying impact energy levels. For the CF/PEI composite, it is observed that after a 5 J impact, the compressive strength remained similar to that of the non-impacted material, considering the variation in the sample's standard deviation. This indicates good structural integrity in areas beyond the impact-induced fracture zone.

It is further observed that, following the 5 J impact, the compressive strength increased compared to the non-impacted material, rising from 95.36 MPa to 109.10 MPa (a 14.41% increase). The 14.41% increase can be attributed to a localized stress redistribution mechanism facilitated by HE. At low energy levels, the HE acts as a high-stiffness interlayer that restricts initial transverse crack propagation. This creates a 'bridge effect' where the impact energy is dissipated into the surrounding matrix through elastic deformation rather than forming critical interlaminar voids. Furthermore, the localized heating during welding may induce beneficial residual compressive stresses at the interface. These stresses, coupled with the absence of significant fiber breakage at 5J, temporarily enhance the laminate's stability against microbuckling during subsequent compression, effectively raising the load-bearing threshold before structural failure. This behavior may also be related to the transfer of impact energy to the surrounding regions of the material, thus reducing the concentration of damage in the impact area, as reported by Cengiz et al. [31]. However, when the composite is subjected to a 30 J impact, the compressive strength decreases to 87.79 MPa (a 7.94% reduction). This indicates that, at this energy level, delamination damage, matrix damage, and fiber failure are enough to significantly compromise the material’s mechanical properties, consistent with observations by Tuo et al. [33] and Qiang et al. [34].

The GF/PEI composite exhibits distinct behavior. The compressive strength of the non-impacted material is 79.55 MPa, which is lower than that of the carbon fiber composite, highlighting the lower intrinsic strength of glass fibers compared to carbon fibers. After a 5 J impact, the GF/PEI compressive strength decreases to 65.80 MPa (a 17.28% reduction), indicating that the glass fiber composite sustains significant damage that compromises its structural integrity even at low impact energy levels. When the impact energy increases to 30 J, the compressive strength of GF/PEI further decreases,

reaching 58.64 MPa (a 26.29% reduction). This highlights the material's tendency to exhibit lower impact resistance and greater susceptibility to distributed damage and degradation of mechanical properties. The FCAI vs. Impact Energy graph (Fig. 4) compares the two materials, indicating that CF/PEI demonstrates superior impact resistance at low energy levels, as previously observed.

However, both composites undergo significant property degradation at high energy levels (30 J), with GF/PEI showing a more pronounced reduction. These results indicate that while CF/PEI is more resistant and tolerant to low-energy impacts, GF/PEI, although capable of broader energy dissipation, experiences a greater loss in structural performance when subjected to high-energy impact loads. This is also attributed to the influence of the HE, which enhanced energy dissipation and reduced internal damage during low-energy impact tests [32]. However, performance loss occurred due to delamination at high energy levels. Table 3 summarizes the parameters observed in the impact tests.

Table 3
Impact parameters on CF/PEI and GF/PEI.

Average data	**CF/PEI 5J**	**GF/PEI 5J**	**CF/PEI 30J**	**GF/PEI 30J**
Absorbed energy (J)	4.71 ± 0,17	4.9 ± 0,01	24.35 ± 0,24	30.57 ± 0,07
Impact energy (J)	5	5	30	30
Impact velocity (m/s)	2.87	2.87	2.70	2.70
Peak force (kN)	1.94 ± 0.02	1.98 ± 0.02	2.84 ± 0.03	5.64 ± 0.12
Peak energy (J)	3,51 ± 0,20	4,90 ± 0,01	9,99 ± 0,60	30,54 ± 0,11

The delamination observed in the ultrasonic images of the CF/PEI and GF/PEI laminates (Figs. 5 and 6, respectively), especially in the central region, indicates the impact site and suggests a failure mechanism. This failure is likely linked to interlaminar delamination caused by modulus mismatches between the layers [35].

To establish a proper baseline, the pristine welded joints were characterized via optical microscopy and ultrasonic mapping. CF/PEI specimens exhibited high consolidation quality with a nominal fiber volume fraction of approximately 50% and low porosity of 0.5%. Ultrasonic images of non-impacted samples (Fig. 5a and 6a) show a uniform color distribution, indicating a high degree of intimate contact and effective polymer interdiffusion across the interface. While GF/PEI showed some localized areas of poorer consolidation (Fig. 6a) compared to CF/PEI, the overall weld line integrity remained sufficient for structural testing. This baseline confirms that the subsequent strength reductions observed were strictly a result of impact-induced damage rather than manufacturing defects.

In both materials, this failure is demonstrated by variations in color and intensity within the ultrasonic images, which are linked to changes in material density and internal integrity. The CF/PEI composite exhibited lower impact resistance, with a concentrated damage area at the center (Fig. 5b), suggesting that the impact caused significant internal discontinuities and localized fractures. The behavior of the CF/PEI composite thus demonstrates reduced impact resistance and more focused damage, likely due to the concentration of impact energy.

In contrast, while more flexible, the GF/PEI composite demonstrates higher impact resistance than CF/PEI, with a smaller fracture area. The ultrasonic images of GF/PEI, both before impact (Fig. 6a) and after impact (Fig. 6d), show areas of poorer consolidation and, for impacted specimens, more extensive delamination throughout the sample structure compared to CF/PEI. This suggests that glass fibers have a higher energy absorption capacity, distributing damage over a larger area—a phenomenon also observed by Deng et al. [36], who reported increased toughness and energy absorption in glass fiber-reinforced composites. This behavior reflects the glass fiber's ability to dissipate impact energy more broadly, though with greater deformation and loss of structural integrity compared to carbon fiber, which demonstrates lower energy absorption but maintains higher structural integrity despite localized fracture damage. Additionally, the HE significantly enhances toughness, improving the laminate’s energy absorption capacity, as observed by Cengiz et al. [31].

The relationship between absorbed energy and impact force further supports these findings. At the 30 J level, GF/PEI absorbed approximately 25.5% more energy than CF/PEI. This higher energy dissipation is attributed to the ductility of glass fibers and a broader distribution of damage, as confirmed by the more extensive delamination seen in ultrasonic imaging compared to the localized failure in carbon fiber samples. Yuan et al. [37] fiber breakage contributes to the dissipation of incident impact energy, a phenomenon that is more frequently observed in carbon fibers than in glass fibers. These results indicate that CF/PEI maintains structural integrity more effectively, even under severe impact conditions.

The relationship between impact energy and the reduction in compressive load, expressed by the ratio Pu/Pmax and illustrated in Fig. 7 (with mean values summarized in Table 4), demonstrates that CF/PEI retains greater structural integrity post-impact than GF/PEI. This suggests the carbon fiber composite is less susceptible to mechanical property degradation. In contrast, GF/PEI, due to the lower inherent strength of glass fibers, undergoes a more significant reduction in load-bearing capacity. The results indicate that CF/PEI exhibits greater resistance to delamination and structural damage across varying energy levels, whereas GF/PEI, while more efficient in energy dissipation, experiences higher structural degradation post-impact. The reduction of deformation and the impact-damaged area serve as evidence of enhanced impact energy absorption in the material [35, 37].

Table 4
Normalized ultimate compression load knockdown.

Laminate	$\varvec{x}$ E_{max} (J)	$\varvec{x}$ P_u/P_{max}
CF/PEI	5	1.15 ± 0.07
	30	0.93 ± 0.19
GF/PEI	5	0.83 ± 0.02
	30	0.73 ± 0.03

3.3 Optical characterization

Figure 8 illustrates optical microscopy mapping of CF/PEI specimens following impact testing at energy levels of 5 J and 30 J. Figure 9 depicts optical microscopy using extended depth-of-field reconstruction for GF/PEI specimens after impact testing at energy levels of 5 J and 30 J. Failure occurred in the central region of all specimens, initiating as delamination across the width and culminating in fiber fracture. This failure pattern is consistent with results reported in the literature [26, 38–40]. Additionally, the impact induced translaminar failures, as indicated by the blue arrows. When comparing CF/PEI and GF/PEI samples, cracks in the fracture region were observed in CF/PEI specimens, likely due to increased delamination that is perpendicular to the compression direction [26, 38, 40, 41].

Comparing Fig. 8(a) with Fig. 8(b), it is observed that the 30 J impact energy caused more significant delamination and fiber rupture compared to the 5 J energy (a). This indicates that impact energy directly influences the extent of weld damage. The HE likely restricted crack propagation perpendicular to the weld direction; however, it also contributed to delamination at the mesh-composite interface [42].

Similarly to the findings shown in Figs. 9(a) and 9(b), increasing the impact energy from 5 J (Fig. 9a) to 30 J (Fig. 9b) resulted in greater damage to the weld region. It is noted that glass fiber exhibits lower impact resistance than carbon fiber, as evidenced by the larger damaged area and fiber fragmentation in Fig. 9(b). The HE seems to have a similar effect to that observed in the CF/PEI composite, restricting crack propagation perpendicular to the weld direction while intensifying delamination at the interface.

SEM images of the sample cross-sections and damage analysis for each impact level were obtained. Figures 10 and 11 clearly illustrate the separation between composite layers. Longitudinal cracks parallel to the fibers indicate either fiber-matrix interfacial debonding or matrix failure between layers, which precedes structural collapse after impact. Transverse rupture of the fiber bundles is also evident, as shown in Fig. 8. While the integrated wire mesh within the composite matrix protects the material against immediate total (transverse) failure, it weakens the adhesion between adjacent laminae, making delamination the dominant failure mode in this region.

According to the literature [43, 44], delamination originates from the bending stiffness mismatch between successive material layers. It is observed that the internal delaminated area is more extensive than the superficial damage zone. During the impact event, the coexistence of compressive stresses at the contact zone and tensile stresses on the opposite face induces matrix failure between fibers, resulting in external cracking and deep interfacial damage [45].

Analysis of Figs. 12 and 13 for the GF/PEI composite reveals matrix crack propagation that intensifies from the outer toward the inner face. It is observed that both radial cracking and delamination processes are more pronounced in the laminae adjacent to the HE surfaces opposite to the impact, a behavior similar to that verified for the CF/PEI. Furthermore, the synergy between different degradation mechanisms in regions near the interfacial debonding zones induces the initiation of further cracking.

At the intersections where radial fractures converge toward the delaminated zones, the matrix exhibits severe damage, resulting in fiber exposure and compromised local structural integrity, as illustrated in Fig. 12. Under higher impact energies (30 J), a more aggressive delamination propagation is observed, corroborating the lower resistance of GF/PEI compared to CF/PEI. This vulnerability is evidenced by fiber fragmentation and a larger damaged area, as shown in Fig. 13.

The apparent contradiction between the high energy absorption (25.5% higher than CF/PEI) and the significant compressive strength reduction (26.29%) in GF/PEI is explained by the material's failure morphology. Unlike the localized fracture in CF/PEI, GF/PEI undergoes extensive matrix cracking and radial fractures that propagate from the outer to the inner face (Figs. 12 and 13). The higher energy absorption is primarily driven by irreversible damage mechanisms, specifically widespread interlaminar debonding and matrix plastic deformation. While SEM images (Figs. 12–13) show less catastrophic fiber breakage than carbon fiber, the synergy between radial cracking and delamination near the HE interfaces compromises the lateral stability of the glass fibers. This leads to premature structural collapse under compression despite the material's superior toughness.

4. Conclusion

This study evaluated the impact resistance of resistance-welded CF/PEI and GF/PEI laminates. The findings reveal that CF/PEI exhibits superior impact resistance across all tested energy levels, while GF/PEI demonstrates a higher energy absorption capacity that results in a broader distribution of damage. A critical performance distinction was observed under low-energy impacts (5J), where CF/PEI displayed a "self-reinforcing" behavior with a 14.41% increase in compressive strength. This phenomenon is attributed to the stainless-steel heating element (HE) acting as a high-stiffness interlayer that redistributes impact energy through elastic dissipation to surrounding regions, effectively preserving the structural integrity of the impact zone. Conversely, although GF/PEI absorbed approximately 25.5% more energy at 30J than CF/PEI, this led to a pronounced 26.29% reduction in load-bearing capacity. This loss in performance is driven by extensive matrix cracking and radial fractures that compromise the lateral stability of the glass fibers, leading to premature structural collapse despite the material's higher

energy dissipation. The inclusion of the HE provides a dual benefit by acting as both a welding agent and a physical barrier to crack propagation perpendicular to the weld. However, its presence also intensifies the tendency for interlaminar delamination at the mesh-composite interface under high-energy impacts. From an engineering perspective, these results suggest that CF/PEI is better suited for primary structures requiring high damage tolerance, such as Urban Air Mobility (UAM) airframes. In contrast, GF/PEI offers advantages for energy-shielding applications, such as Electric Vehicle (EV) battery enclosures, where maximum energy dissipation is prioritized to protect internal components. Finally, these results reinforce the viability of electrical resistance welding for structural thermoplastic composites. Future research should focus on optimizing welding parameters (current, time, and pressure) to minimize delamination, addressing the moisture sensitivity of the PEI matrix, and exploring surface treatments to enhance interfacial adhesion for high-load applications.

Declarations

Acknowledgements

This work was supported by National Council for Scientific and Technological Development – CNPq (processes 404875/2023-8, 306576/2020-1 and 312200/2021-8).

Funding Declaration

The authors disclose that this research was supported by the National Council for Scientific and Technological Development (CNPq). This funding source had no role in the study design, data collection, analysis, interpretation of data, or the writing of the manuscript.

Ethics, Consent to Participate, and Consent to Publish declarations: Not applicable.

Author Contribution

J. F, T.S.R and L.F.B wrote the main manuscript text; J.F and L.F.B prepared all figures 1-13. All authors reviewed the manuscript.

Data Availability

The datasets generated during and/or analysed during the current study are available from the corresponding author on reasonable request.

References

1. Calabrese L, Cicala G, Di Bella G et al. Optimisation of ultrasonic welding process of carbon/epoxy composites using Nylon-based or PES thermoplastic interlayers. Compos B Eng. 2024;275.

2. Rubino F, Parmar H, Mancia T et al. Ultrasonic welding of glass reinforced epoxy composites using thermoplastic hybrid interlayers. Compos Struct. 2023;314.
3. Yang J, Oliveira JP, Li Y et al. Laser techniques for dissimilar joining of aluminum alloys to steels: A critical review. J. Mater. Process. Technol. Elsevier Ltd; 2022.
4. Bianchi I, Forcellese A, Mancia T, et al. Process parameters effect on environmental sustainability of composites FFF technology. Mater Manuf Processes. 2022;37(5):591–601.
5. Khan R. Fiber bridging in composite laminates: A literature review. Compos. Struct. Elsevier Ltd; 2019.
6. Rohart V, Lebel LL, Dubé M. Effects of environmental conditions on the lap shear strength of resistance-welded carbon fibre/thermoplastic composite joints. Compos B Eng. 2020;198.
7. Saleh MN, Soutis C. Recent advancements in mechanical characterisation of 3D woven composites. Mech Adv Mater Mod Process. 2017;3(1).
8. Hu Y, He Z, Xuan H. Impact resistance study of three-dimensional orthogonal carbon fibers/bmi resin woven composites. Materials. 2020;13(19):1–17.
9. Farahani RD, Dubé M. Novel Heating Elements for Induction Welding of Carbon Fiber/Polyphenylene Sulfide Thermoplastic Composites. Adv Eng Mater. 2017;19(11).
10. Kropka M, Muehlbacher M, Neumeyer T, et al. From UD-tape to Final Part – A Comprehensive Approach Towards Thermoplastic Composites. Procedia CIRP. 2017;66:96–100.
11. Yang Y, Boom R, Irion B, et al. Recycling of composite materials. Chem Eng Process. 2012;51:53–68.
12. Brassard D, Dubé M, Tavares JR. Modelling resistance welding of thermoplastic composites with a nanocomposite heating element. J Compos Mater. 2021;55(5):625–39.
13. Zhao T, Palardy G, Villegas IF, et al. Mechanical behaviour of thermoplastic composites spot-welded and mechanically fastened joints: A preliminary comparison. Compos B Eng. 2017;112:224–34.
14. Yousefpour A, Hojjati M, Immarigeon JP. Fusion bonding/welding of thermoplastic composites. J Thermoplast Compos Mater. 2004. pp. 303–41.
15. Li X, Zhang T, Li S, et al. The effect of cooling rate on resistance-welded CF/PEEK joints. J Mater Res Technol. 2021;12:53–62.
16. Xiong X, Zhao P, Ren R et al. Enhanced resistance-welding hybrid joints of titanium alloy/thermoplastic composites using a carbon-nanotube lamina. Diam Relat Mater. 2020;101.
17. Zhao P, Zhang Z, Li Y et al. Resistance welding of thermoplastic composites via a novel carbon nanofilm implant. Mater Lett. 2022;328.
18. Tijs BHAH, Doldersum MHJ, Turon A et al. Experimental and numerical evaluation of conduction welded thermoplastic composite joints. Compos Struct. 2022;281.
19. Al Omari AS, Al-Athel KS, Arif AFM et al. Experimental and computational analysis of low-velocity impact on carbon-, glass- and mixed-fiber composite plates. J Compos Sci. 2020;4(4).
20. Falzon B, Tan W. Predicting Impact Damage, Residual Strength and Crashworthiness of Composite Structures. SAE Int J Mater Manuf. 2016;9(3):718–28.

21. Riccio A, Di Felice G, Saputo S, et al. Stacking sequence effects on damage onset in composite laminate subjected to low velocity impact. Procedia Eng. Elsevier Ltd; 2014. pp. 222–9.
22. Farooq U, Myler P. Prediction of load threshold of fibre-reinforced laminated composite panels subjected to low velocity drop-weight impact using efficient data filtering techniques. Results Phys. 2015;5:206–21.
23. De Fenza A, Petrone G, Pecora R, et al. Post-impact damage detection on a winglet structure realized in composite material. Compos Struct. 2017;169:129–37.
24. Reis JF, Abrahao ABM, Costa ML, et al. Assessment of the interlaminar strength of resistance-welded PEI/carbon fibre composite. Weld Int. 2018;32(2):149–60.
25. Lan X, Hao S, Liu L, et al. Macroscale bending large-deformation and microbuckling behavior of a unidirectional fiber-reinforced soft composite. J Compos Mater. 2020;54(2):243–57.
26. Conejo Ldos, Santos S, de Ribeiro LF. Reconsolidation effect on impact, compression after impact and thermal properties of poly (aryl ether ketone) composites for aeronautical applications. J Thermoplast Compos Mater. 2023;36(6):2562–81.
27. Ismail KI, Sultan MTH, Shah AUM, et al. Low velocity impact and compression after impact properties of hybrid bio-composites modified with multi-walled carbon nanotubes. Compos B Eng. 2019;163:455–63.
28. Boria S, Scattina A, Belingardi G. Impact behavior of a fully thermoplastic composite. Compos Struct. 2017;167:63–75.
29. Mandegarian S, Hojjati M. Experimental investigation on the effects of stainless-steel mesh reinforcing layers on low-velocity impact response of hybrid thermoplastic glass fiber composites. J Compos Mater. 2024;58(16):1887–904.
30. Sakthivel M, Vijayakumar S, Ramnath BV. Investigation on Mechanical and Thermal Properties of Stainless Steel Wire Mesh-Glass Fibre Reinforced Polymer Composite. Silicon. 2018;10(6):2643–51.
31. Cengiz A, Yıldırım İM, Avcu E. Flexural and low velocity impact behaviour of hybrid metal wire mesh/carbon-fibre reinforced epoxy laminates. Compos Commun. 2024;46.
32. Sakthivel M, Vijayakumar S. Influence of stainless-steel wire mesh on the mechanical behaviour in a glass-fibre-reinforced epoxy composite. Materiali Tehnologije. 2017;51(3):455–61.
33. Tuo H, Lu Z, Ma X, et al. An experimental and numerical investigation on low-velocity impact damage and compression-after-impact behavior of composite laminates. Compos B Eng. 2019;167:329–41.
34. Qiang X, Wang T, Xue H, et al. Study on Low-Velocity Impact and Residual Compressive Mechanical Properties of Carbon Fiber–Epoxy Resin Composites. Materials. 2024;17:15.
35. Seamone A, Davidson P, Waas AM et al. Low velocity impact and compression after impact of thin and thick laminated carbon fiber composite panels. Int J Solids Struct. 2024;292.
36. Deng Y, Li X, Hu X et al. Experimental investigation on low-velocity impact response of carbon/glass hybrid S-shaped foldcore sandwich structure. Thin-Walled Struct. 2022;180.

37. Yuan B, Tan B, Hu Y, et al. Improving impact resistance and residual compressive strength of carbon fibre composites using un-bonded non-woven short aramid fibre veil. Compos Part Appl Sci Manuf. 2019;121:439–48.
38. Shah SZH, Megat-Yusoff PSM, Karuppanan S et al. Compression and buckling after impact response of resin-infused thermoplastic and thermoset 3D woven composites. Compos B Eng. 2021;207.
39. Xu X, Zhou Z, Hei Y, et al. Improving compression-after-impact performance of carbon-fiber composites by CNTs/thermoplastic hybrid film interlayer. Compos Sci Technol. 2014;95:75–81.
40. Sun XC, Hallett SR. Failure mechanisms and damage evolution of laminated composites under compression after impact (CAI): Experimental and numerical study. Compos Part Appl Sci Manuf. 2018;104:41–59.
41. Hart KR, Chia PXL, Sheridan LE, et al. Comparison of Compression-After-Impact and Flexure-After-Impact protocols for 2D and 3D woven fiber-reinforced composites. Compos Part Appl Sci Manuf. 2017;101:471–9.
42. Wei D, Gu Y, Zhu H et al. Influence of Electrical Heating Metal Mesh and Power Density on Resistance Welding of Carbon Fiber/PEEK Composite. Polym (Basel). 2022;14(13).
43. Gemi L, Sinan Şahin Ö, Akdemir A. Experimental investigation of fatigue damage formation of hybrid pipes subjected to impact loading under internal pre-stress. Compos B Eng. 2017;119:196–205.
44. Gemi L, Kara M, Avci A. Low velocity impact response of prestressed functionally graded hybrid pipes. Compos B Eng. 2016;106:154–63.
45. Gemi L, Kayrıcı M, Uludağ M, et al. Experimental and statistical analysis of low velocity impact response of filament wound composite pipes. Compos B Eng. 2018;149:38–48.

Figures



Figure 1

Impact testing machine setup and specimen positioning.

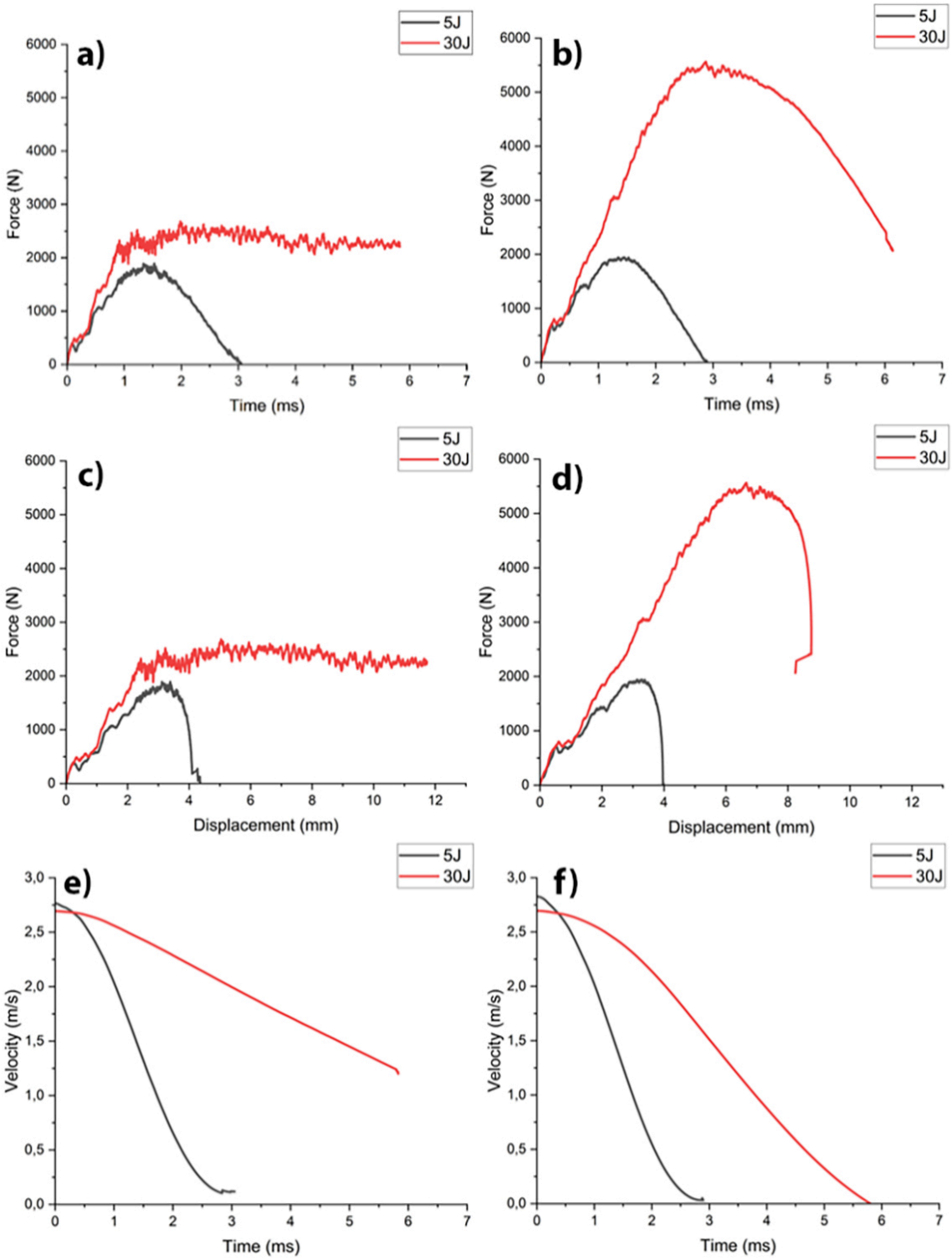


Figure 2

Force-time, force-displacement, and velocity-time graphs for CF/PEI (a, c, and e) and GF/PEI (b, d, and f) composites.

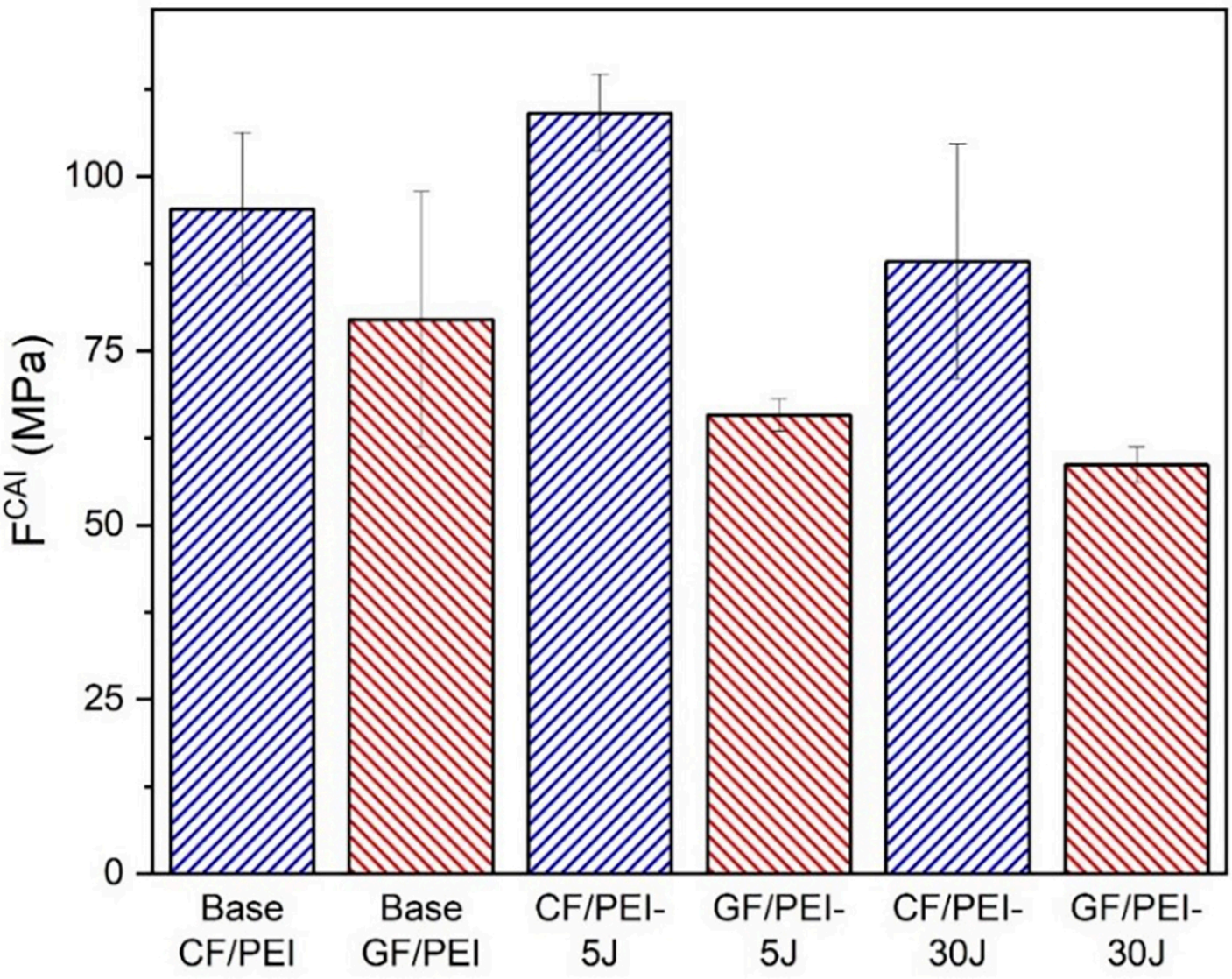


Figure 3

F_{CAI} applied to welded composite materials.

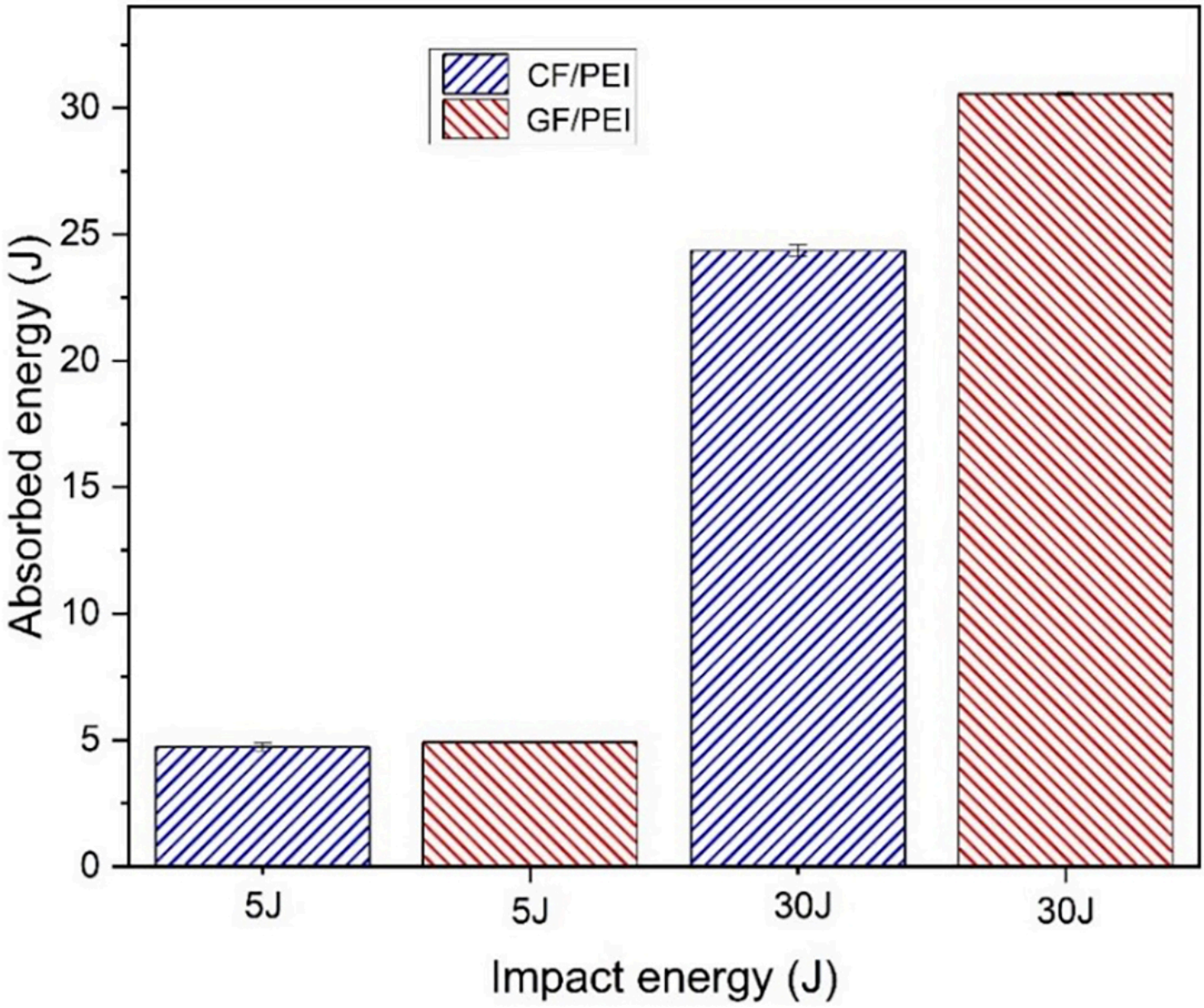


Figure 4

The F_{CAI} vs. Impact Energy graph.

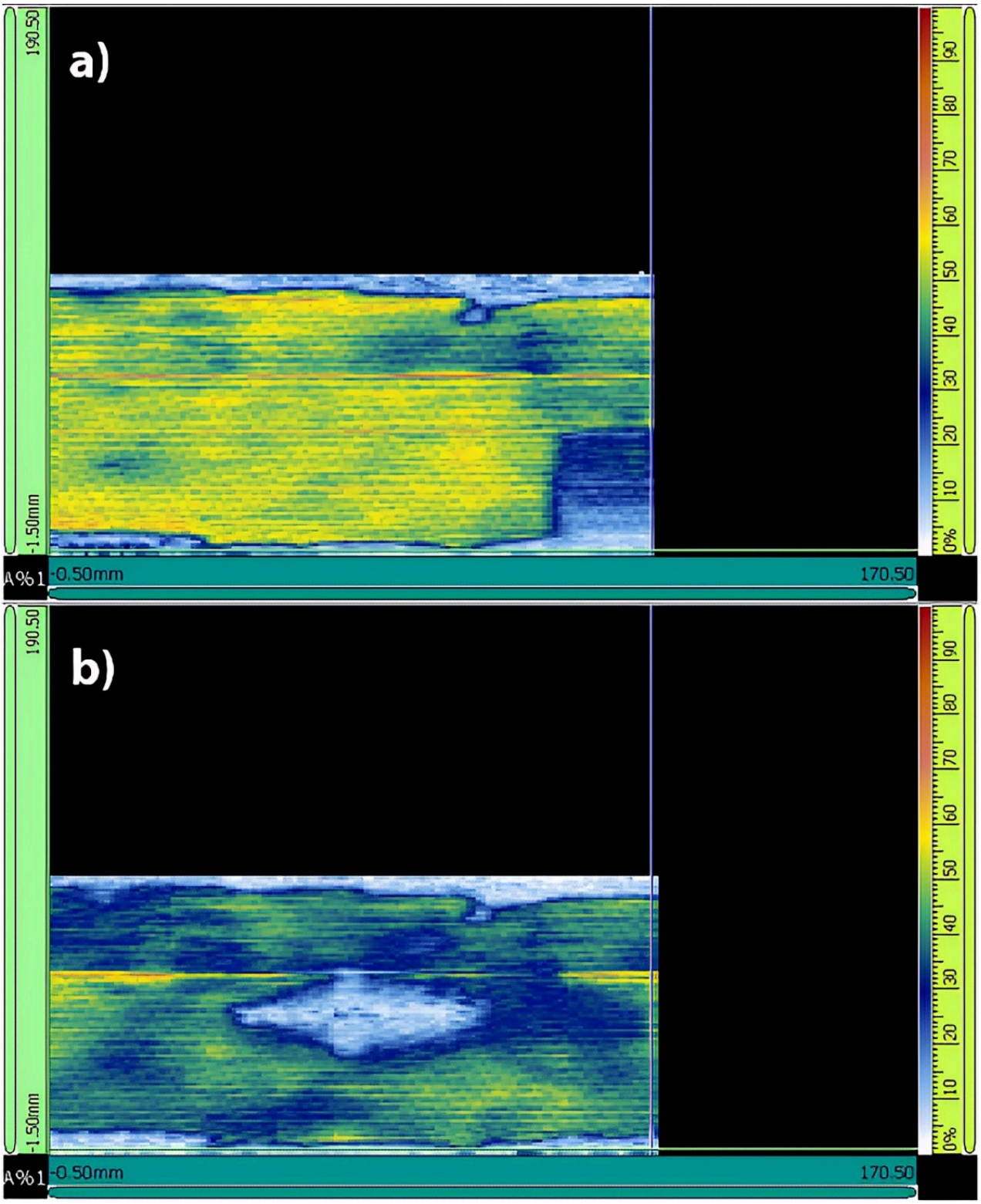


Figure 5

Ultrasonic imaging of CF/PEI (a) before and (b) following impact.

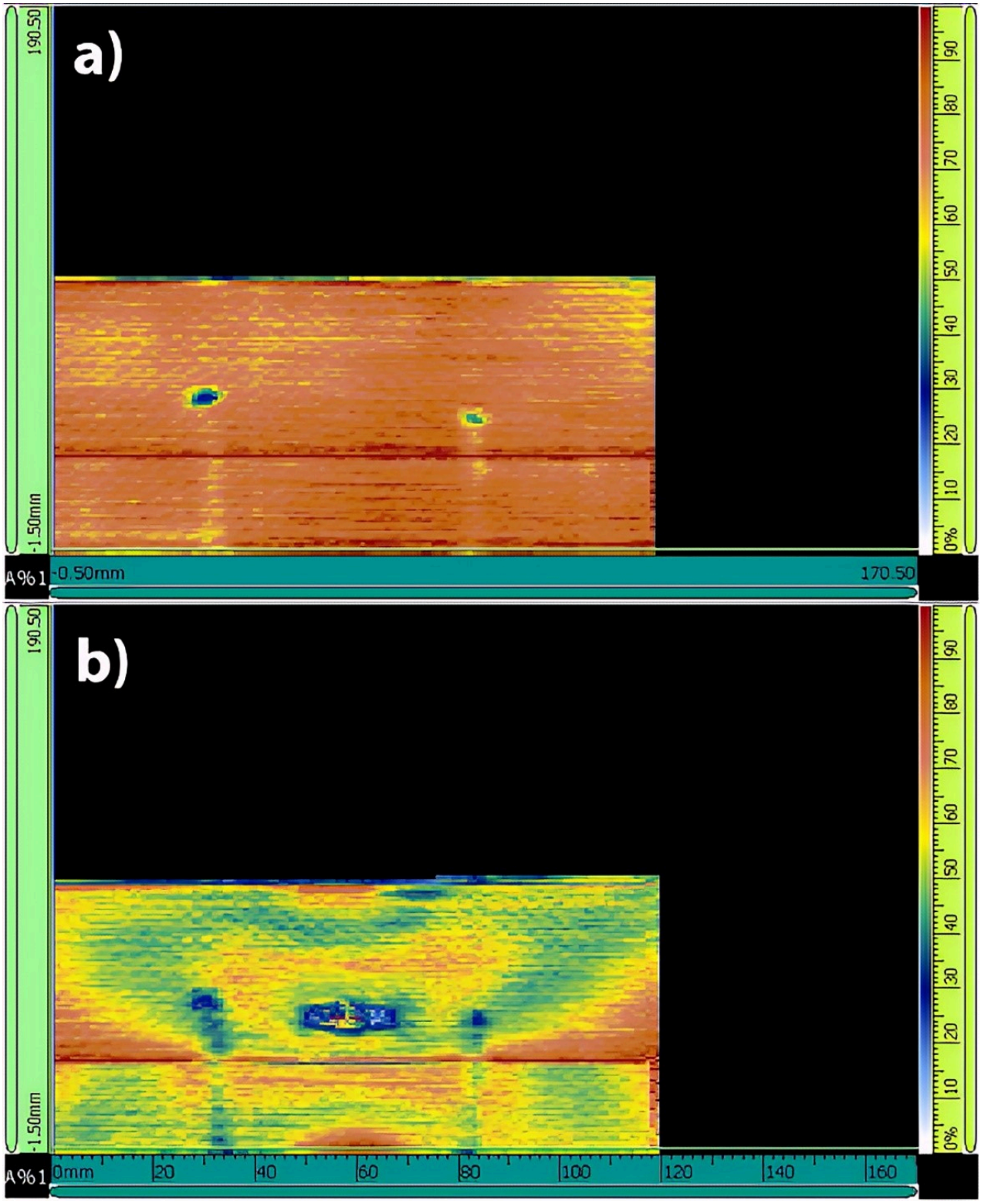


Figure 6

Ultrasonic imaging of GF/PEI (a) before and (b) following impact.

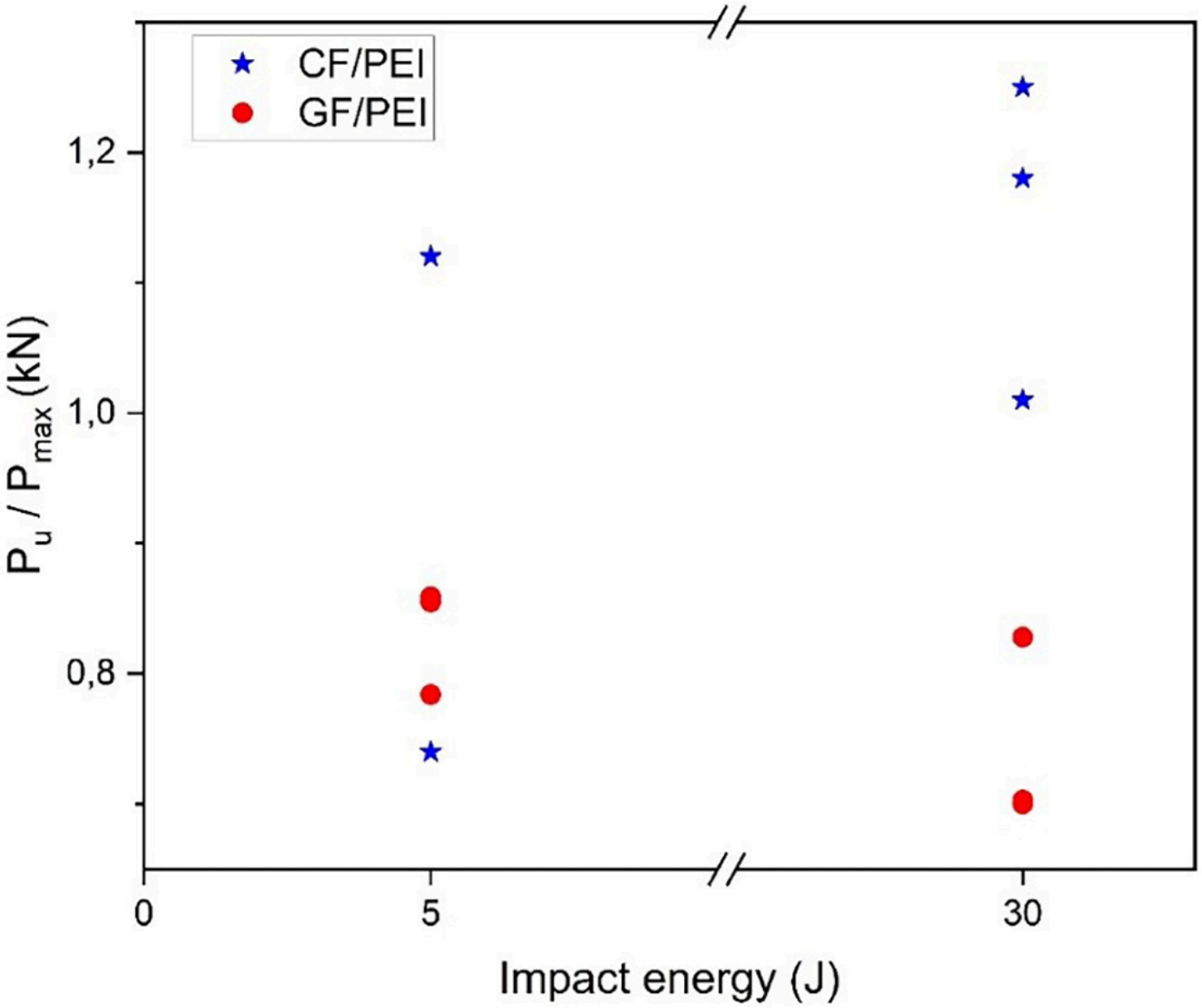


Figure 7

Relationship between impact energy and reduction of compressive load.

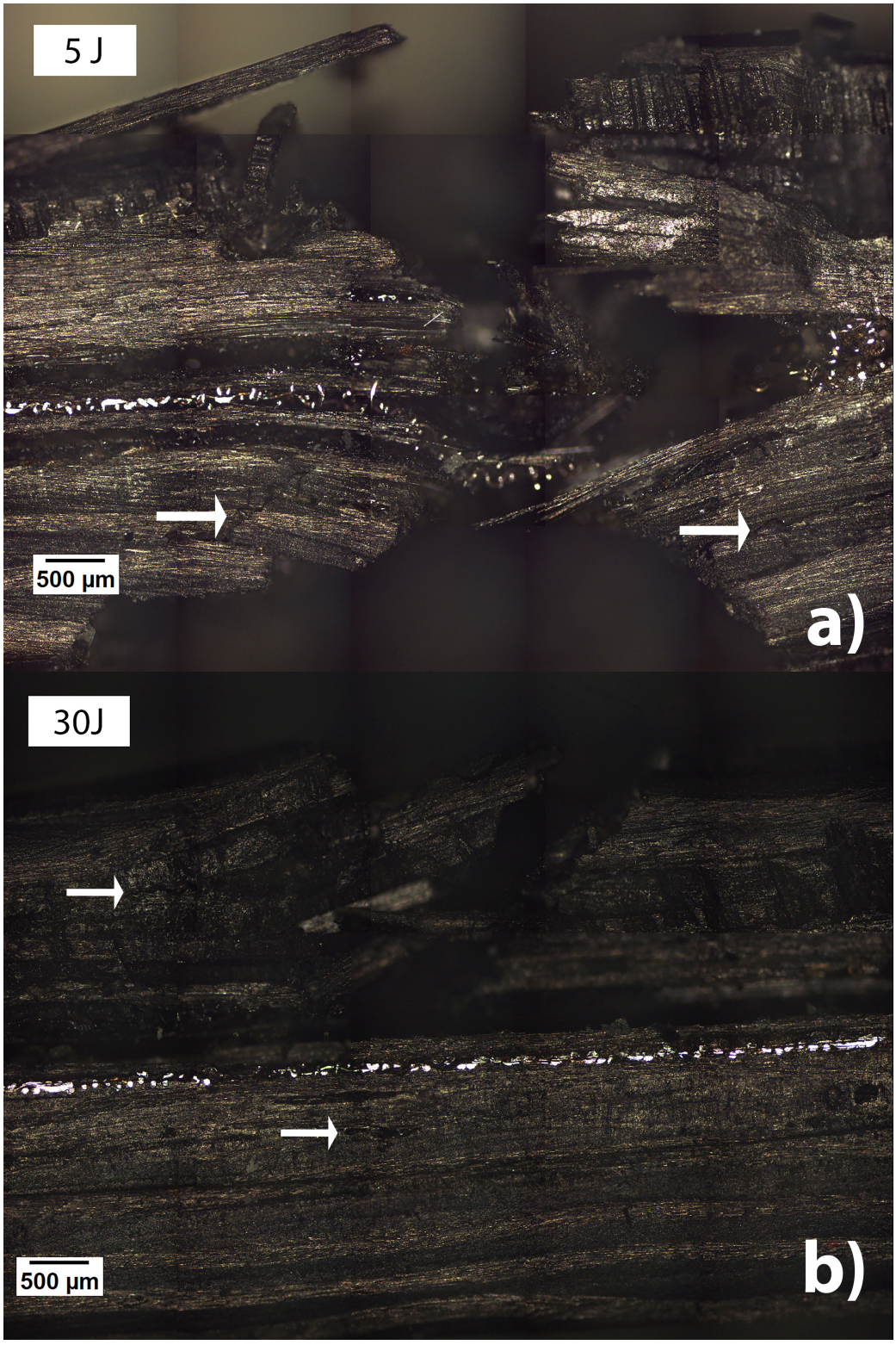


Figure 8

Optical microscopy of the fracture region using image mapping for CF/PEI: (a) 5 J and (b) 30 J.

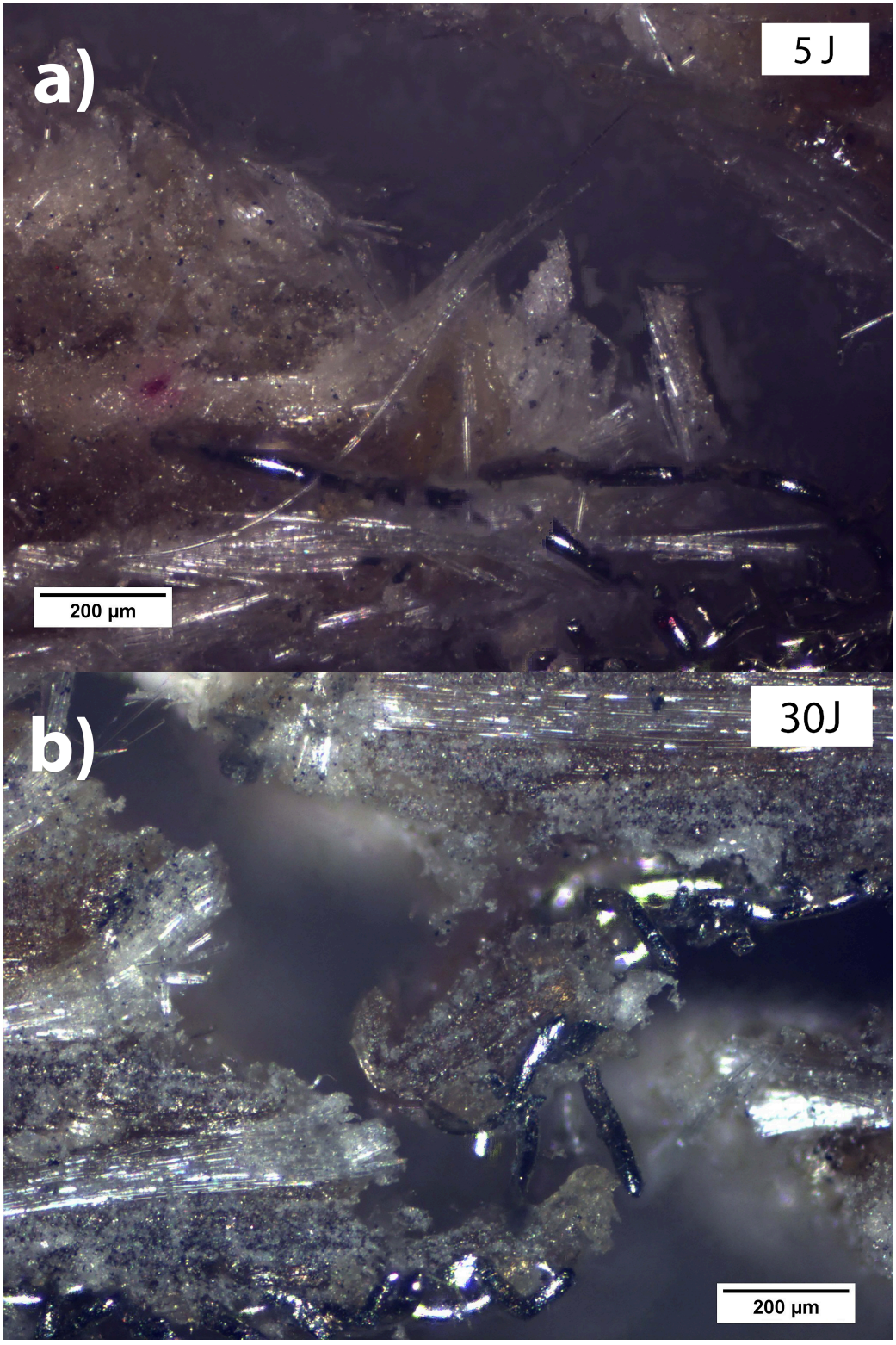


Figure 9

Optical microscopy using extended depth-of-field reconstruction of GF/PEI: (a) 5 J and (b) 30 J.

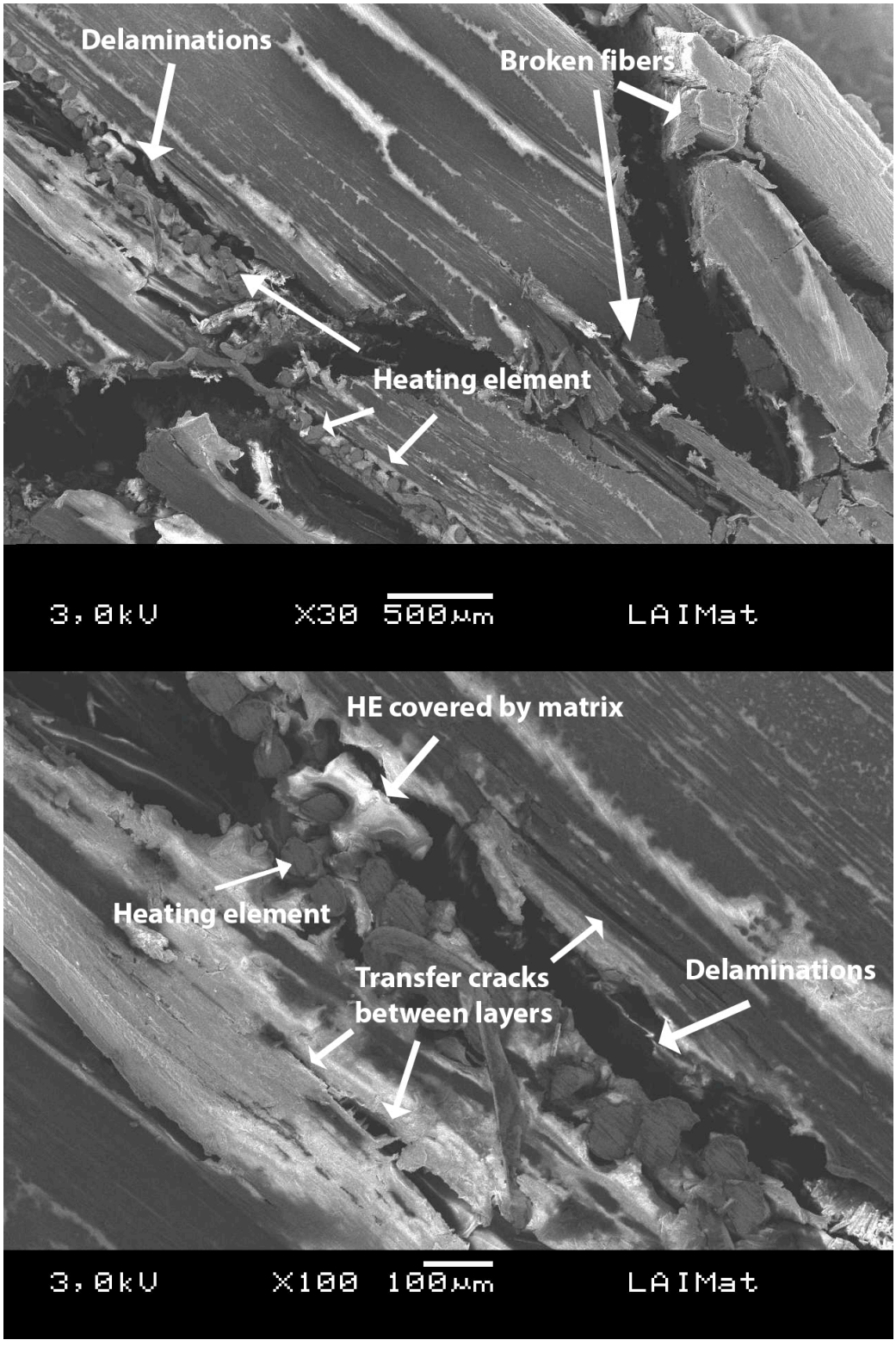


Figure 10

SEM image of damage formed on CF/PEI specimens subject to impact at 5J.

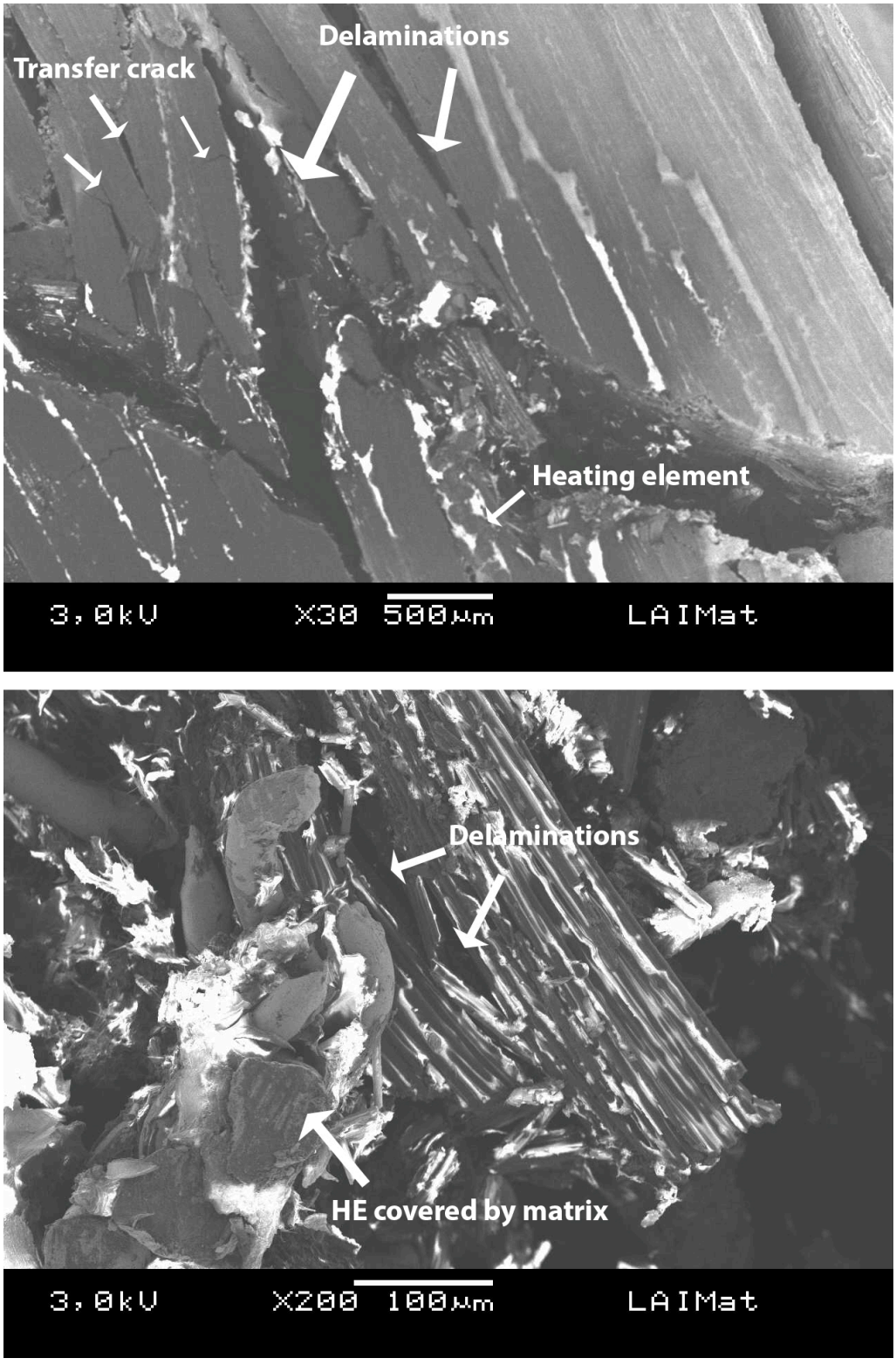


Figure 11

SEM image of damage formed on CF/PEI specimens subject to impact at 30J.

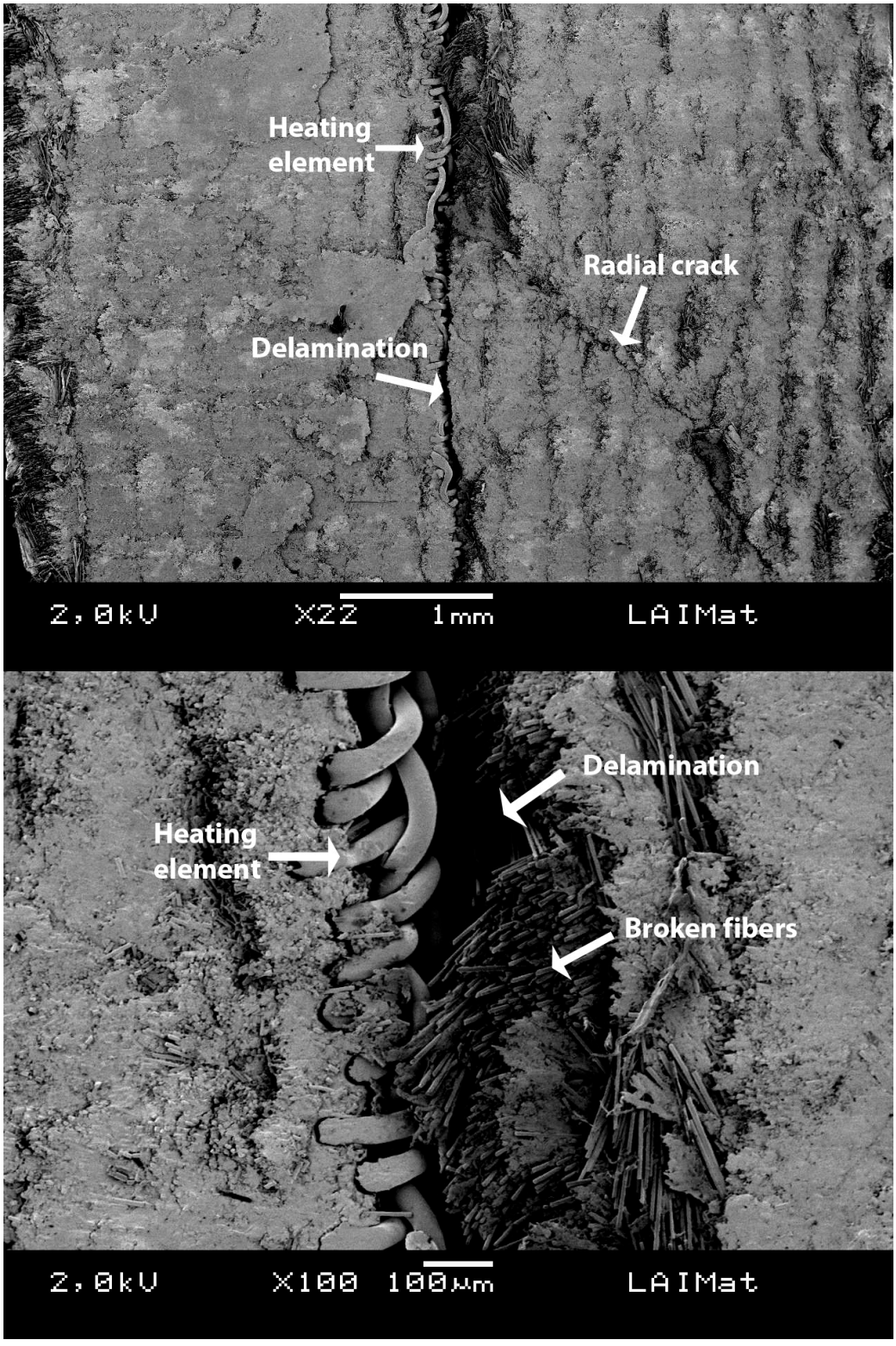


Figure 12

SEM image of damage formed on GF/PEI specimens subject to impact at 5J.

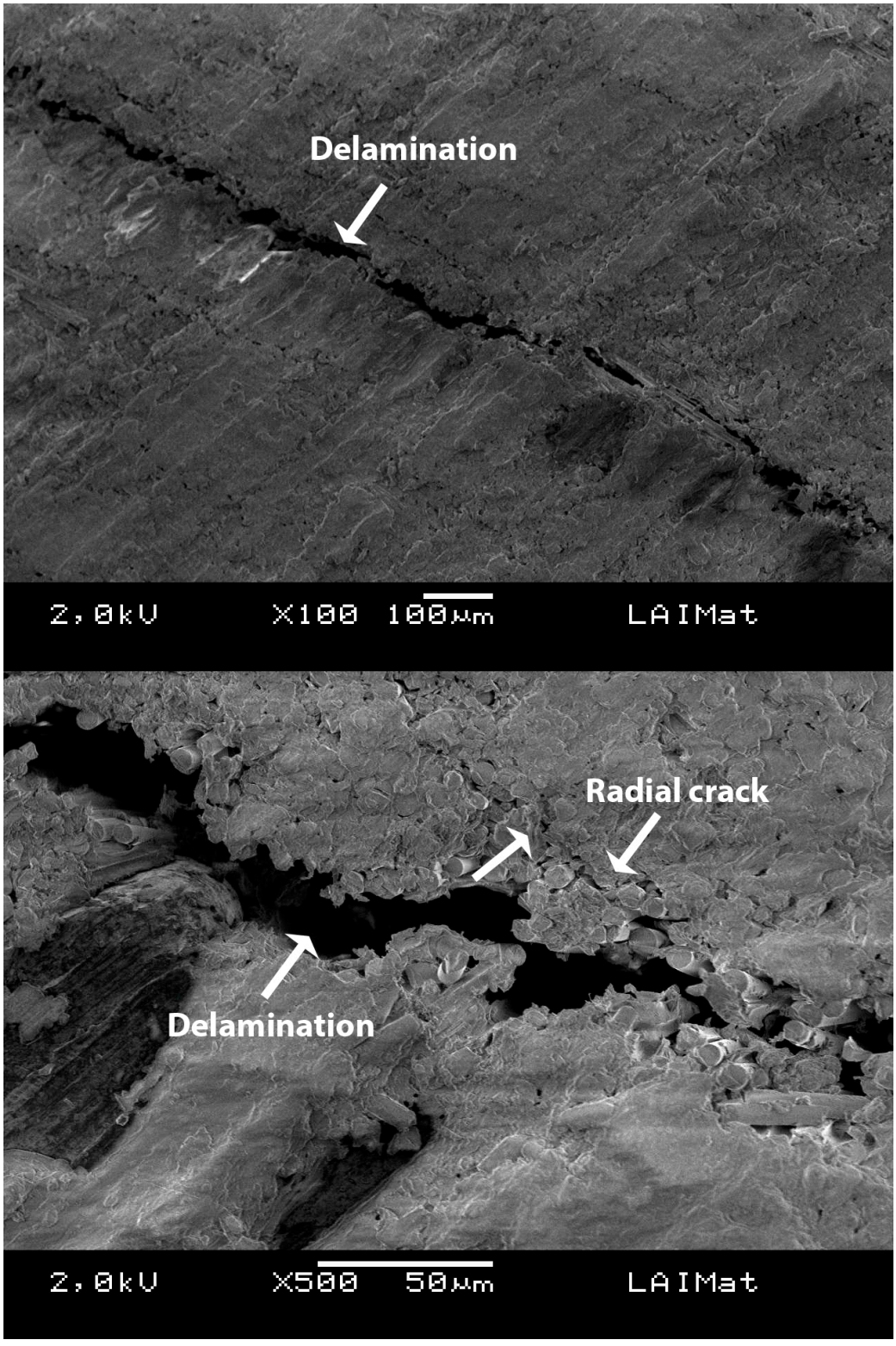


Figure 13

SEM image of damage formed on GF/PEI specimens subject to impact at 30J.